

# Anomalous second magnetization peak in 12442-type $\text{RbCa}_2\text{Fe}_4\text{As}_4\text{F}_2$ superconductors

Xiaolei Yi(易晓磊)<sup>1,2</sup> Xiangzhuo Xing(邢相灼)<sup>1,3,\*</sup> Yan Meng(孟炎)<sup>1,4</sup> Nan Zhou(周楠)<sup>1,5</sup> Chunlei Wang(王春雷)<sup>2</sup> Yue Sun(孙悦)<sup>1,†</sup> and Zhixiang Shi(施智祥)<sup>1,‡</sup>

<sup>1</sup>*School of Physics, Southeast University, Nanjing 211189, China*

<sup>2</sup>*College of Physics and Electronic Engineering, Xinyang Normal University, Xinyang 464000, China*

<sup>3</sup>*School of Physics and Physical Engineering, Qufu Normal University, Qufu 273165, China*

<sup>4</sup>*School of Physical Science and Intelligent Engineering, Jining University, Qufu 273155, China*

<sup>5</sup>*Key Laboratory of Materials Physics, Institute of Solid State Physics, HFIPS, Chinese Academy of Sciences, Hefei, 230031, China*

The second magnetization peak (SMP) appears in most superconductors, and is crucial for the understanding of vortex physics as well as the application. Although it is well known that the SMP is related to the type and quantity of disorder/defects, the mechanism has not been universally understood. In this work, we selected three stoichiometric superconducting  $\text{RbCa}_2\text{Fe}_4\text{As}_4\text{F}_2$  single crystals with identical superconducting critical temperature  $T_c \sim 31$  K and similar self-field critical current density  $J_c$ , but with different amounts of disorder/defects, to study the SMP effect. It is found that only the sample S2 with moderate disorder/defects shows significant SMP effect. The evolution of the normalized pinning force density  $f_p$  demonstrates that the dominant pinning mechanism changes from the weak pinning at low temperatures to strong pinning at high temperatures. The microstructure study for sample S2 reveals some expanded  $\text{Ca}_2\text{F}_2$  layers and dislocation defects in  $\text{RbFe}_2\text{As}_2$  layers. The normalized magnetic relaxation results indicate that the SMP is strongly associated with the elastic to plastic (E-P) vortex transition. As temperature increases, the SMP gradually evolves into a step-like shape and then becomes a sharp peak near the irreversibility field similar to what is usually observed in low-temperature superconductors. Our findings connect the low field SMP of high-temperature superconductors and the high field peak of low temperature superconductors, revealing the possible universal origin related to the E-P phase transition.

## I. INTRODUCTION

Research of vortex dynamics in superconductors is of great significance for fundamental research as well as for technical applications [1, 2]. One of the most interesting phenomena of vortex dynamics is the second magnetization peak (SMP) effect in the magnetization hysteresis loop that has been widely observed in many type-II superconductors, particularly in high-temperature superconductors. Until now, various theoretical models have been proposed to understand the SMP effect, including softening of vortex lattice [3, 4], vortex lattice structure phase transition [5–7], a crossover from elastic to plastic (E-P) vortex transition [8, 9], and vortex order-disorder transition [10], etc. However, the mechanism is still unclear, and there is still an ongoing research in recently discovered superconductors [11–14].

For most high-temperature superconductors, the parent compounds are non-superconducting, and superconductivity is generally achieved by extra element doping [15, 16]. As a consequence, equivalent or nonequivalent chemical doping inevitably introduces defects and inhomogeneities that can be regarded as scattering centers for quasiparticles [17]. It is known that the nature of vortex is highly sensitive to the type and quantity of defect. In general, the vortex motion in high-temperature supercon-

ductors is determined by the strong pinning attributed to sparse nanometer-sized defects [18] and the weak collective pinning by atomic-scaled defects [1, 19]. Therefore, all the inhomogeneities, defects, and scattering centers will act together as the pinning sources, complicating the behavior of the vortices. In this sense, the stoichiometric superconducting materials provide an unique platform to study the effect of disorder/defect on the vortex dynamics, free from the additional extrinsic effects introduced by chemical substitutions.

Recently, a new type of stoichiometric iron-based superconductors (IBSs)  $\text{ACa}_2\text{Fe}_4\text{As}_4\text{F}_2$  ( $A = \text{K}, \text{Rb}, \text{Cs}$ ), namely, 12442-type was discovered by the intergrowth of 1111-type  $\text{CaFeAsF}$  and 122-type  $\text{AFe}_2\text{As}_2$  ( $A = \text{K}, \text{Rb}, \text{Cs}$ ) [20], consisting of double  $\text{Fe}_2\text{As}_2$  layers separated by insulating  $\text{Ca}_2\text{F}_2$  layers. Such unique double  $\text{Fe}_2\text{As}_2$  layered structure resembles the double  $\text{CuO}_2$  layers in cuprate superconductors  $\text{La}_{2-x}\text{Sr}_x\text{CaCu}_2\text{O}_6$  and  $\text{Bi}_2\text{Sr}_2\text{CaCu}_2\text{O}_{8+\delta}$  [21, 22]. It manifests a quasi two-dimensional (2D) electronic behavior with a significant anisotropy of normal-state resistivity  $\rho_c/\rho_{ab} > 100$ , and a large upper critical field ( $H_{c2}$ ) anisotropy  $\sim 8$  [23, 24], comparable to those of cuprate superconductors. The inelastic neutron scattering study has revealed a 2D spin resonant mode with downward dispersion [25], also resembling the behavior observed in cuprates. Moreover, the pronounced resistive tail of superconducting transition under magnetic field and relatively low irreversibility field ( $H_{\text{irr}}$ ) indicate that the coupling between double  $\text{Fe}_2\text{As}_2$  layers is weaker than most IBSs [23, 26, 27]. On the other hand, the SMP effect and

\* xzxing@qfnu.edu.cn

† sunyue@seu.edu.cn

‡ zxshi@seu.edu.cn

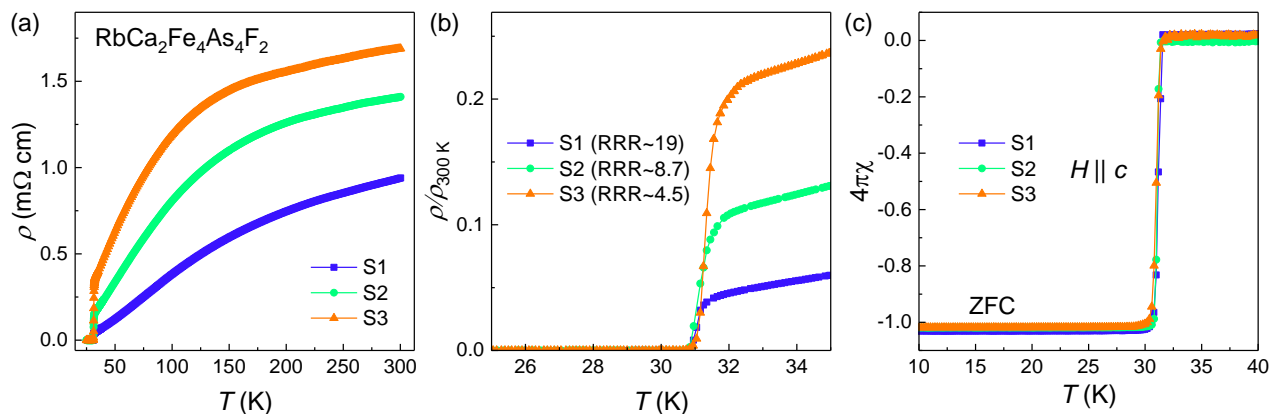


FIG. 1. (a) The temperature dependence of the in-plane resistivity  $\rho(T)$  of three selected  $\text{RbCa}_2\text{Fe}_4\text{As}_4\text{F}_2$  single crystals. (b) Magnification of superconducting transition region normalized to the resistivity at 300 K. (c) Temperature dependence of susceptibility under an applied magnetic field of 5 Oe with  $H \parallel c$ .

the critical current density  $J_c$  in the 12442 system are strongly sample-dependent. For example, the self-field  $J_c$  of  $\text{KCa}_2\text{Fe}_4\text{As}_4\text{F}_2$  single crystal is almost one order of magnitude higher than that of  $\text{Rb/CsCa}_2\text{Fe}_4\text{As}_4\text{F}_2$  [23, 27, 28], while a unique SMP effect that shows a non-monotonic variation with temperature is observed in  $\text{RbCa}_2\text{Fe}_4\text{As}_4\text{F}_2$  single crystals [28]. To avoid the additional effects introduced by chemical doping, the stoichiometric  $A\text{Ca}_2\text{Fe}_4\text{As}_4\text{F}_2$  ( $A = \text{K, Rb, Cs}$ ) single crystals with unique intergrowth structure can be regarded as a good candidate to study the vortex dynamics, especially the main factors of governing SMP phenomenon.

In this paper, we study the vortex dynamics of  $\text{RbCa}_2\text{Fe}_4\text{As}_4\text{F}_2$  based on three selected single crystals with identical superconducting transition temperature  $T_c \sim 31$  K but with different levels of disorder/defect. It is found that the one with moderate disorder/defects shows a pronounced non-monotonic SMP effect. Some expanded  $\text{Ca}_2\text{F}_2$  layered and dislocation defects of  $\text{RbFe}_2\text{As}_2$  layers are found by microstructure study. Furthermore, magnetic relaxation measurement reveals that the SMP is strongly associated with the E-P vortex transition. The systematic evolution of SMP indicates the complex vortex motion of the 12442 system, which provides insights into the vortex dynamics for novel superconductors with intergrowth structure.

## II. EXPERIMENTAL DETAILS

Single crystals of  $\text{RbCa}_2\text{Fe}_4\text{As}_4\text{F}_2$  were grown by the self-flux method, details of the crystal growth are given in our previous report [24]. X-ray diffraction (XRD) was characterized via a commercial Rigaku diffractometer with  $\text{Cu } K\alpha$  radiation. Elemental analysis was performed by a scanning electron microscope equipped with

an energy dispersive x-ray spectroscopy probe. Structure and elemental analysis reveal that only  $(002l)$  ( $l$  diffraction peaks are detected and the average atom ratios are almost consistent with the nominal stoichiometry [24, 28]. The in-plane electrical resistivity was carried out by the standard four-probe method on a Physical Property Measurement System (PPMS, Quantum Design). Magnetization measurement was performed by the VSM (vibrating sample magnetometer) option of PPMS. The values of  $J_c$  are calculated using the Bean mode  $J_c = 20\Delta M/[a(1-a/3b)]$  [29], where  $\Delta M = M_{\text{down}} - M_{\text{up}}$ ,  $M_{\text{down}}$  and  $M_{\text{up}}$  are the magnetization measured with decreasing and increasing applied field, respectively,  $a$  and  $b$  are sample widths ( $a < b$ ). The normalized magnetic relaxation rate,  $S(=|\text{dln}M/\text{dln}t|)$ , was measured by tracing the decay of magnetization with time  $M(t)$  due to creep motion of vortices for one hour, where  $t$  is the time from the moment when the critical state is prepared. The cross-sectional observations were investigated by aberration-corrected high-resolution transmission electron microscopy (TEM, Titan Themis3 G2 300) on the thin specimen (thickness  $\sim 50$  nm) prepared by a focused ion beam instrument (Helios NanoLab G3 UC).

## III. RESULTS AND DISCUSSION

The in-plane resistivity  $\rho(T)$  curves for three  $\text{RbCa}_2\text{Fe}_4\text{As}_4\text{F}_2$  single crystals (named by S1, S2, and S3) are shown in Fig. 1(a). All three samples exhibit proximate metal conductive behavior and coherent-incoherent transition in the middle temperature region, which is commonly observed in 12442-type IBSs [20, 30, 31]. The values of residual resistivity ratio (RRR), characterizing the level of disorder/defect and defined as  $\rho(300 \text{ K})/\rho(32.5 \text{ K})$ , are estimated to be  $\sim 19$  for sample

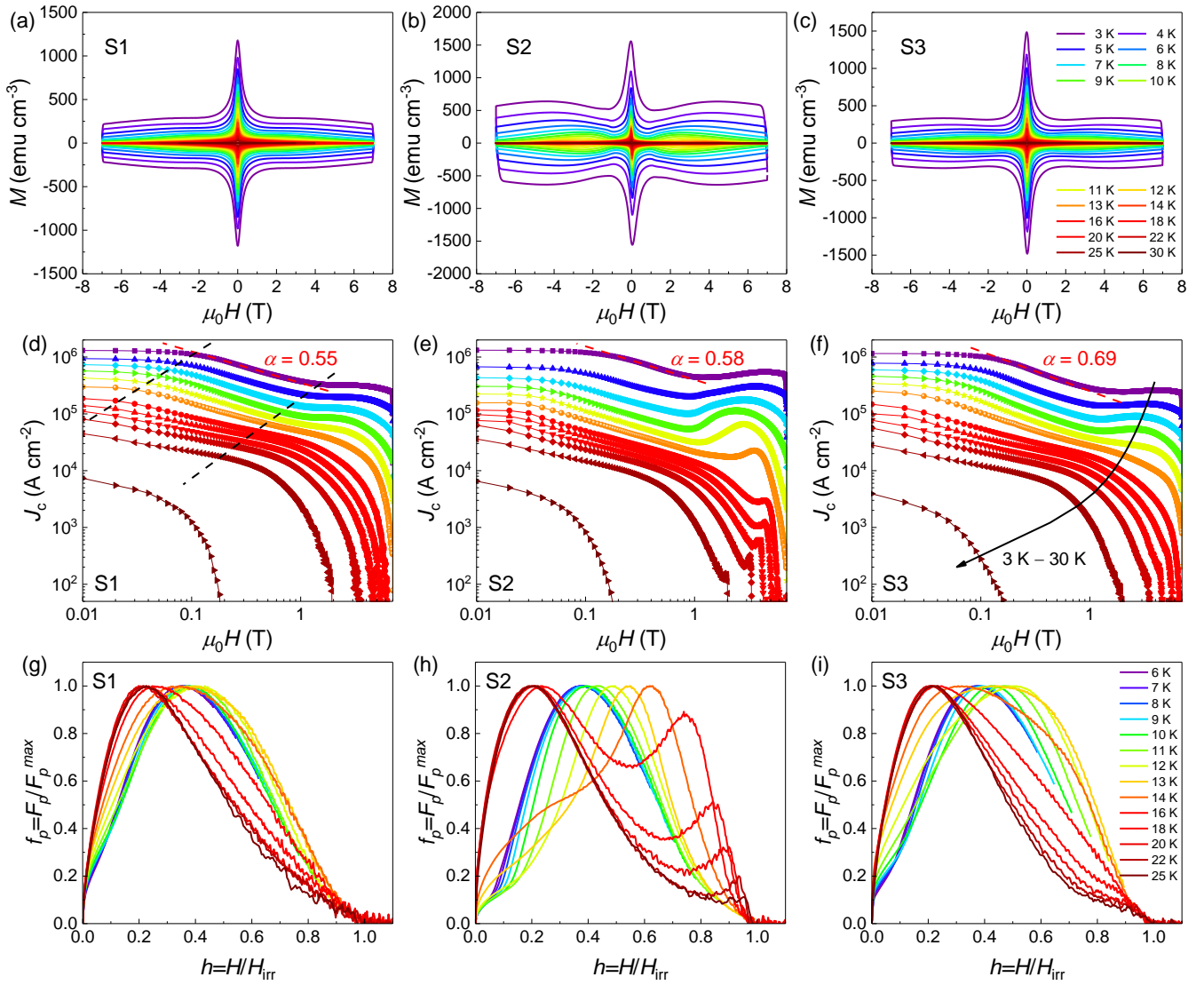


FIG. 2. (a)-(c) Magnetization hysteresis loops at various temperatures ranging from 3 to 30 K for sample S1, S2, and S3, respectively. (d)-(f) The corresponding field dependence of critical current density at constant temperatures calculated by using the Bean model. (g)-(i) The scaling of the normalized pinning force density  $f_p = F_p / F_p^{\max}$  for different temperatures as a function of the reduced field  $h = H / H_{\text{irr}}$ .

S1,  $\sim 8.7$  for sample S2, and  $\sim 4.5$  for sample S3, respectively. The superconducting transition temperatures  $T_c$  determined by the zero resistivity are almost identical with a value of 31 K, regardless of the RRR values. This indicates that the disorder/defects only destroy local superconductivity and have little effect on  $T_c$ . Superconductivity was also confirmed by the susceptibility measurement with zero-field-cooling (ZFC) model, as shown in Fig. 1(c). The onsets of diamagnetism are in good agreement with the resistivity data. The sharp superconducting transition width  $\Delta T_c$ , defined as the temperature difference between 10% and 90% of susceptibility, is less than 1 K for all crystals, indicating the homogeneous

distribution of disorder/defects.

To study the effect of disorder/defect on the critical current density, we measured the magnetization hysteresis loops at various temperatures ranging from 3 to 30 K for the three selected crystals, as shown in Figs. 2(a)-(c). The symmetric loops suggest that the bulk pinning rather than surface or geometrical barriers is dominant. What deserves more attention is the pronounced SMP observed in the sample S2, which is obviously different from the other two crystals with more or less disorder/defects. Such difference can also be detected from the field dependence of  $J_c$  calculated using the Bean model [29] (see Figs. 2(d)-(f)). As seen, the values of the self-field  $J_c$  for

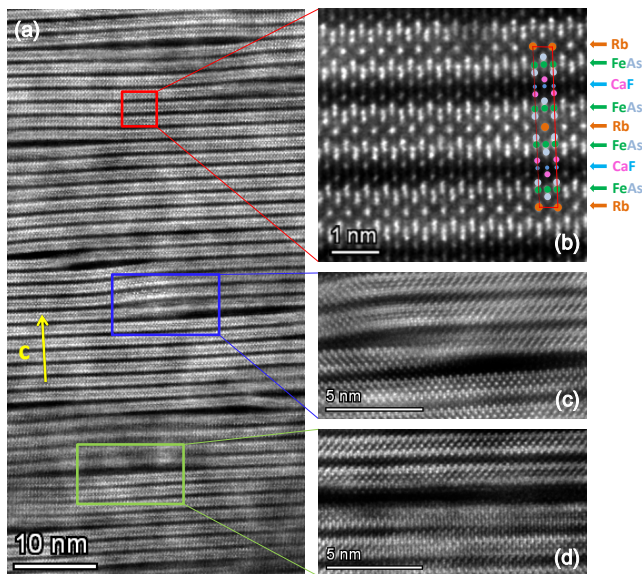


FIG. 3. (a) The microstructures of  $\text{RbCa}_2\text{Fe}_4\text{As}_4\text{F}_2$  single crystal S2 investigated by STEM. (b) High resolution STEM image around regular lattice structure, and atomic arrangements are demonstrated. (c) A type of dislocation defects observed in  $\text{RbFe}_2\text{As}_2$  layer, and stretched lattice in the upper right corner. (d) Another type of expanded  $\text{Ca}_2\text{F}_2$  layered defects.

three crystals are almost the same, slightly larger than  $10^6 \text{ A cm}^{-2}$  at 3 K.  $J_c$  changes little at low fields, which can be associated with single-vortex region. With increasing magnetic field,  $J_c$  follows a power-law behavior  $J_c \propto H^\alpha$  with  $\alpha = 0.55$  for sample S1, 0.58 for sample S2, and 0.69 for sample S3, respectively. Such power-law behavior is also observed in most IBSSs, which can be attributed to the sparse strong point pinning by sparse nano-sized defects [18, 32]. In general, due to the addition of random point defects by chemical doping or irradiation, the level of disorder/defect in the nanoscale increases, and the  $\alpha$  value decreases gradually, as revealed in  $\text{H}^+$ -irradiated  $\text{GdBa}_2\text{Cu}_3\text{O}_{7-\delta}$  and Ni doped  $\text{CaKFe}_4\text{As}_4$  [33, 34]. Therefore, the different values of  $\alpha$  indicate the different levels of defect in three crystals.

Depending on the magnetic field strength, the behavior of  $J_c(H)$  with SMP is generally divided into several regimes: (I) a low-field regime associated with the single-vortex regime; (II) a power law dependence  $J_c \propto H^\alpha$  related to strong pinning centers; (III) a SMP regime related to random disorder and usually related to a crossover from E-P relaxation of vortex lattice; and (IV) a high-field regime characterized by a fast drop in  $J_c(H)$  [9]. The magnetic field  $H_{\text{sp}}$  at which the SMP appears usually decreases with increasing temperature in most of the type-II superconductors. Noticeably,  $H_{\text{sp}}$  of sample S2 decreases at first, then increases with increasing temperature, and finally decreases with a steep

transition adjacent to  $H_{\text{irr}}$  [28], which can be seen more clearly in Fig. 5. However, the other two samples present unobvious or faded SMP characteristics at low temperatures. Therefore, it is plausible to expect that the SMP effect in  $\text{RbCa}_2\text{Fe}_4\text{As}_4\text{F}_2$  is closely related to the level of disorder/defect.

To gain more insight into the underlying pinning mechanisms, the pinning force ( $F_p = \mu_0 H \times J_c$ ) is calculated. As proposed by Dew-Hughes [35], the pinning mechanism does not change with temperature if the normalized pinning force  $f_p = F_p/F_p^{\text{max}}$  at different temperatures can be scaled into a unique curve by the reduced field  $h = H/H_{c2}$ , where  $F_p^{\text{max}}$  is the maximum pinning force, and  $H_{c2}$  is the upper critical field. However, the upper critical field is generally too high to be obtained in high-temperature superconductors, so the irreversibility field  $H_{\text{irr}}$  is widely used in cuprates and IBSSs [36–38]. The deviation from the scaling usually suggests the change in vortex-lattice period or the various size of pinning centers. In Figs. 2(g)-(i), we present the  $f_p$  vs  $h = H/H_{\text{irr}}$  for three crystals.  $H_{\text{irr}}$  is determined from  $J_c(H)$  curves with the criterion of  $J_c = 30 \text{ A cm}^{-2}$  at high temperatures, or extrapolating to  $J_c = 0$  in the  $J_c^{1/2}$  vs  $H$  at low temperatures. Except from the SMP in S2,  $f_p(h)$  shows similar behavior in the three crystals. At low temperatures, the peaks of  $f_p(h)$  are located at  $h_{\text{max}} \sim 0.4-0.5$ . Similar results have been observed in other superconductors such as  $\text{Ba}_{0.68}\text{K}_{0.32}\text{Fe}_2\text{As}_2$  ( $h_{\text{max}} \sim 0.43$ ) [39],  $\text{BaFe}_{1.9}\text{Ni}_{0.1}\text{As}_2$  ( $h_{\text{max}} \sim 0.4$ ) [40, 41], and  $\text{Ba}_{0.66}\text{K}_{0.32}\text{BiO}_{3+\delta}$  ( $h_{\text{max}} \sim 0.47$ ) [42]. According to Dew-Hughes model [35], the present case of  $h_{\text{max}} < 0.5$  is suggestive of  $\delta l$ -type pinning, which arises from a spatial variation in the mean free path of charge carriers, and the pinning is due to the presence of a large density of point-like defect centers whose dimensions are smaller than the intervortex distance. Besides, the peaks in the low field region are located at  $h_{\text{max}} \sim 0.2$ , which is the characteristic of surface strong pinning, such as the planar defects. Obviously, the characteristic of two  $f_p(h)$  peaks is more obvious in sample S2 with the SMP. Therefore, the vortex pinning in  $\text{RbCa}_2\text{Fe}_4\text{As}_4\text{F}_2$  at low temperatures mainly comes from the weak collective pinning at high magnetic field, while it is mainly dominated by the strong pinning at high temperatures.

Because of the non-monotonic temperature dependence of  $H_{\text{sp}}$  at  $T > 9 \text{ K}$  in sample S2 [28], the  $f_p(h)$  curves affected by SMP diverge gradually and cannot be scaled. When it reaches the maximum point of  $H_{\text{sp}}$  near 16 K, the  $f_p(h)$  curve shows two peaks in the low and high field regions, respectively. In addition to scaling peak at low  $h$ , the  $f_p(h)$  peak induced by SMP effect at high temperatures moves gradually to  $H_{\text{irr}}$ , and reduces quickly with the decrease of  $f_p$ . The step-like transition approaching to  $H_{\text{irr}}$  was also reported in  $\text{NbSe}_2$  [43], optimally doped  $\text{Ba}_{1-x}\text{K}_x\text{BiO}_3$  [44], and untwinned  $\text{YBa}_2\text{Cu}_3\text{O}_y$  [45], and it is generally understood as the vortex melting transition.

In order to understand the origin of vortex pinning

and the type of defect in  $\text{RbCa}_2\text{Fe}_4\text{As}_4\text{F}_2$ , the cross-sectional microstructures of the typical sample S2 were explored by high resolution TEM measurement. A typical layered structure with light and dark stripes is observed, as shown in Fig. 3(a). The white stripes in Fig. 3(b) correspond to the Rb and  $\text{Fe}_2\text{As}_2$  layers, while the dark stripes correspond to the  $\text{Ca}_2\text{F}_2$  layers. The complete lattice structure and atomic arrangement of  $\text{RbCa}_2\text{Fe}_4\text{As}_4\text{F}_2$  are demonstrated by the colored spheres. Microstructural investigations in stoichiometric 1144-type  $\text{CaKFe}_4\text{As}_4$  superconductors have revealed defects of fine-sized stacking fault of  $\text{CaFe}_2\text{As}_2$  and/or  $\text{KFe}_2\text{As}_2$  layers as well as the lattice mismatch stress inside the grains [11, 46, 47]. However, neither linearly grown single layers nor step-like stacking fault layers can be visible evidently in  $\text{RbCa}_2\text{Fe}_4\text{As}_4\text{F}_2$ . It also seems reasonable that the inter and intra double  $\text{Fe}_2\text{As}_2$  layers have different symmetries. It is impossible for 1111- and 122-type structures to form stacking faults in the same layer or ladder-like structure. But it is interesting to find two other types of unique defects: (i) large number of obviously expanded  $\text{Ca}_2\text{F}_2$  layers with various width shown in Fig. 3(d), and (ii) obvious dislocations existing in the same layer of  $\text{RbFe}_2\text{As}_2$  shown in Fig. 3(c). The torsional dislocation in the  $\text{RbFe}_2\text{As}_2$  layer seems to be accompanied by the stretched  $\text{Ca}_2\text{F}_2$  layers on both sides. All these exhibit significant lattice stress [23], which may be the main reason for the irregular light and dark change in Fig. 3(a) and the obvious stretched lattice in the upper right corner of Fig. 3(c). It has been reported that there is weak anisotropic  $J_c$  in 12442 system with  $J_c^{H\parallel ab} < J_c^{H\parallel c}$  [23, 27], which is obviously different from 1144 system with significantly anisotropic  $J_c$  and  $J_c^{H\parallel ab} > J_c^{H\parallel c}$  [11, 46, 48, 49]. In  $\text{CaKFe}_4\text{As}_4$ , fine-sized planar defects of  $\text{CaFe}_2\text{As}_2$  and/or  $\text{KFe}_2\text{As}_2$  layers along  $ab$  plane act as pinning centers for vortices when  $H\parallel ab$ , and significantly increase  $J_c$ . While for  $\text{RbCa}_2\text{Fe}_4\text{As}_4\text{F}_2$  single crystals, appropriate amounts of lamellar defects with smaller width and thinner thickness, the lattice mismatch stress, and chemical inhomogeneity, work together as pinning centers in both directions, showing relatively smaller critical current anisotropy and novel SMP phenomenon.

It has been proposed that the SMP effect is generally present in samples with moderate pinning strength, possibly associated with a crossover from E-P transition [9, 34]. To further verify and explore the origin of the SMP in the high magnetic field region, measurement of the normalized magnetic relaxation rate,  $S(=|\text{dln}M/\text{dln}t|)$ , is performed as a function of temperature for several applied magnetic fields on sample S2. Fig. 4(a) shows the magnetic field dependence of the normalized relaxation rate. With increasing magnetic field,  $S$  at low temperatures first drops to the value of  $\sim 0.03$ , followed by a gradual increasing, which is attributed to successive change of vortex bundle size from a single vortex to small bundle and large bundle regimes [1]. At high temperatures,  $S$  increases rapidly. The val-

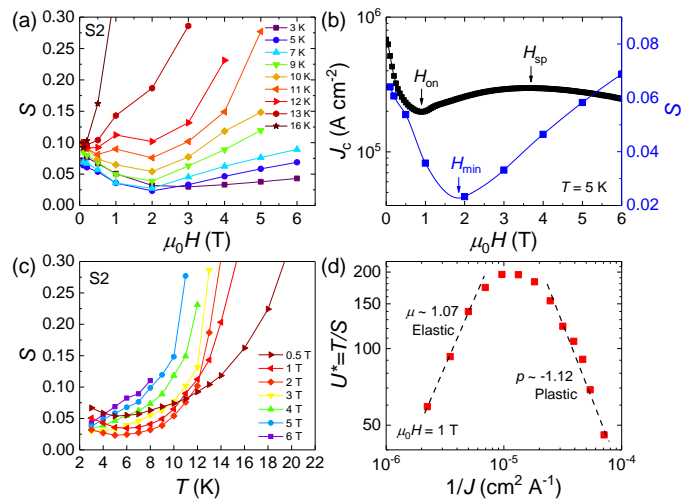


FIG. 4. Measurement of magnetic relaxation of sample S2. (a) The magnetic field dependence of the normalized relaxation rate  $S$  under different temperatures. (b) Field dependence of critical current density  $J_c$  and relaxation rate  $S$  at  $T = 5$  K. (c) The temperature dependence of the normalized relaxation rate  $S$  under different magnetic fields. (d) Inverse current density dependence of effective pinning energy  $U^*$  at  $\mu_0 H = 1$  T.

ues are much larger than those of conventional superconductors, but comparable to those 11-type [50], 122-type [9], and 1144-type IBSS [34], exhibiting a universal "giant flux creep". It has been observed that the minimum in the  $S(H)$  curves is generally accompanied with the presence of SMP phenomenon [6, 7, 51, 52]. In order to probe the correlation between the creep rate and SMP,  $S(H)$  curves at selective temperatures are also plotted together with the  $J_c(H)$  curve at the same temperatures. As shown in Fig. 4(b), the minimum  $H_{\min}$  in the  $S(H)$  curve is located between the onset ( $H_{\text{on}}$ ) of SMP and the second peak position ( $H_{\text{sp}}$ ). This feature has also been found in  $\text{FeSe}_{0.5}\text{Te}_{0.5}$  [53],  $\text{Ba}(\text{Fe}_{0.93}\text{Co}_{0.07})_2\text{As}_2$  [9],  $\text{Ca}_{0.8}\text{La}_{0.2}\text{Fe}_{1-x}\text{Co}_x\text{As}_2$  [38], and many superconductors with SMP, in agreement with the picture of E-P vortex transition. Fig. 4(c) shows the temperature dependence of magnetic relaxation rate  $S$  under different magnetic fields. A plateau in the intermediate-temperature range with a high vortex creep rate  $S \sim 0.05$  is detected, as previously observed in  $\text{YBa}_2\text{Cu}_3\text{O}_{7-\delta}$  [2],  $\text{SmFeAsO}_{0.9}\text{F}_{0.1}$  [54],  $\text{Ba}(\text{Fe}_{1-x}\text{Co}_x)_2\text{As}_2$  [55],  $\text{Ca}_{0.8}\text{La}_{0.2}\text{Fe}_{1-x}\text{Co}_x\text{As}_2$  [38], and  $\text{FeSe}_{0.6}\text{Te}_{0.4}$  [56], which can be interpreted by the collective creep theory [2].

It is well known that the IBSS usually exhibit a giant flux creep rate, and it can be well described by the collective pinning theory, which is characterized by the current density  $J$  dependence of the activation energy  $U$ . The effective activation energy as a function of current density  $J$  is given by interpolation formula  $U(J)$

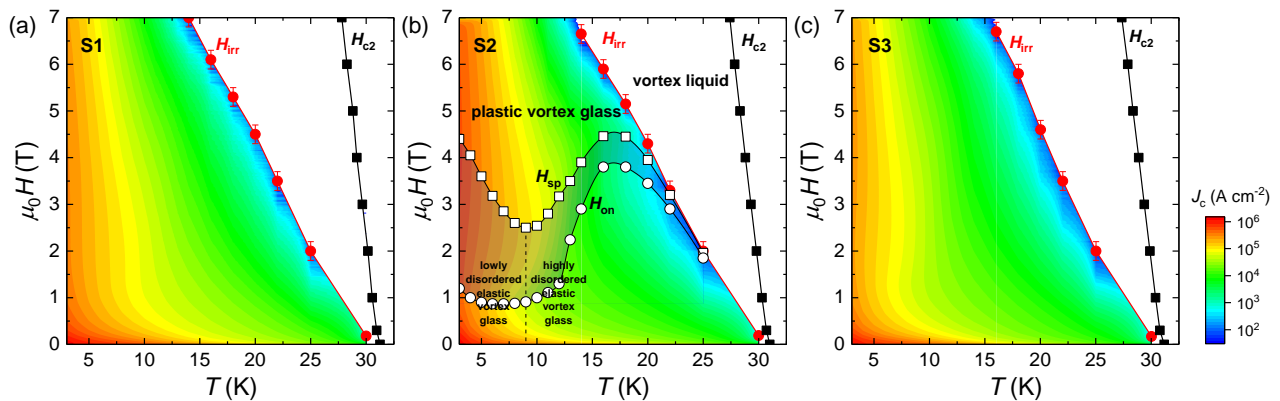


FIG. 5. Vortex phase diagrams of three selected  $\text{RbCa}_2\text{Fe}_4\text{As}_4\text{F}_2$  single crystals (a) S1, (b) S2, and (c) S3 with different disorder/defect levels, respectively.

$= (U_0/\mu)[(J_{c0}/J)^\mu - 1]$ , where  $U_0$  is the collective pinning barrier in the absence of flux creep,  $J_{c0}$  is the temperature-dependent critical current density in the absence of flux creep, and  $\mu$  is the vortex pinning regime-dependent glassy exponent [1]. In this theory, the glassy exponent  $\mu$  is related to the vortex-bundle size, and it is predicted as  $\mu = 1/7, 3/2$  or  $5/2, 7/9$  for single-vortex, small-bundle, and large-bundle regimes, respectively [1, 19]. By defining the effective pinning barrier  $U^* = T/S$  and combining the interpolation formula,  $U^*$  can be calculated as:  $U^* = U_0 + \mu T \ln(t/t_0) = U_0 (J_{c0}/J)^\mu$ . Thus, the slope in the double logarithmic plot of  $U^*$  vs  $1/J$  represents the value of  $\mu$ , as manifested in Fig. 4(d). To avoid the effect of fast relaxation at high temperatures and high magnetic fields,  $\mu \sim 1.07$  was evaluated under 1 T in low temperature region. This value is the prediction of single-vortex and small-bundle regimes, indicating the contributions from different pinning types. On the other hand, the evaluated negative slopes  $p \sim -1.12$  are also observed at small  $J$  region, which is often denoted as plastic creep scenario with  $p \sim -0.5$  [8]. It should be pointed out that E-P vortex phase transition is a necessary condition for the occurrence of SMP, but not a sufficient factor. For example, it exists in FeSe single crystals without SMP [50], but is absent in the different Co doped  $\text{CaFe}_2\text{As}_2$  whose vortex dynamics are plastic creeping rather than collective creep model [57]. In addition, for the Co doped  $\text{BaFe}_2\text{As}_2$  in the very underdoped and overdoped region, the SMP effect becomes invisible or very weak [55]. Therefore, the existence of the E-P crossover as well as the moderate disorder can lead to the emergence of a typical SMP. In other words, the combination of sparse strong pinning centers and dense weak pinning centers is beneficial to SMP.

From the above experimental results, we depict the vortex phase diagrams of three  $\text{RbCa}_2\text{Fe}_4\text{As}_4\text{F}_2$  single crystals shown in Figs. 5(a)-(c). The color contour represents the critical current density  $J_c$ . The orange and

yellow range with  $J_c > 10^5 \text{ A cm}^{-2}$  extends to a high magnetic field region, indicating its excellent current-carrying capacity.  $H_{\text{irr}}$  is the irreversibility field, and the upper critical field  $H_{c2}$  is determined by the resistive measurement with criterions of 90% of the normal state resistivity  $\rho_n$  under magnetic field. Above  $H_{c2}(T)$  line, the system enters into the normal state. Below it, it changes into vortex liquid state, and a unique vortex slush phase exists near the vortex glass temperature [28]. In the vortex phase diagram of sample S2,  $H_{\text{sp}}(T)$  divides the critical current region into two parts beneath  $H_{\text{irr}}(T)$ . Below  $H_{\text{sp}}(T)$ , the vortex motion can be well interpreted with the collective vortex motion. With increasing magnetic field, the flux creep becomes faster, and the system enters into the plastic creep regime. The elastic vortex glass region can be divided into the lowly and highly disordered vortex glass state by abnormal point around 9 K (represented by the dotted line) [28]. In fact, the actual E-P transition occurred at the characteristic field  $H_{\text{min}}$  between  $H_{\text{sp}}$  and  $H_{\text{on}}$  [38].

For the non-monotonic behavior of  $H_{\text{sp}}$ , it is found that the width of the SMP as marked by black shadow decreases gradually with increasing temperature. At low temperatures, E-P phase transition has been confirmed by the results of normalized magnetic relaxation. The dense weak pinning centers dominate the collective pinning. The pinning potential increases first and then decreases with magnetic field. In the high temperature region, strong pinning centers are dominant, and the pinning potential decreases monotonously. At the same time, it should be accompanied by the change of magnetic relaxation mode. In the region of low temperature and low field, since the elastic creep of flux bundle is dominant, there is less disorder and stronger rigidity. On the other hand, in the high temperature and low field region, the flux softens gradually. It changes to the plastic creep of single vortex with increasing disorder, and is characterized by the increase of creep. Therefore, the

SMP in the high temperature region is still dominated by E-P phase transition, and the width of SMP decreases monotonously with increasing temperature. When approaching the  $H_{\text{irr}}(T)$  line, the vortex phase transition from elastic to plastic is very close to the first-order flux melting transition in low temperature superconductors in the high field region. The SMP gradually evolves into a step-like transition and then becomes a peak shape. We suspect that the step-like behavior may be a crossover from the second-order (E-P transition) to first-order transition (vortex melting transition). Certainly, this calls for further investigations both experimentally and theoretically [43]. It is noted that the E-P phase transition reflected by this non-monotonic SMP in the 12442 system just connects the SMP of high temperature superconductors at low fields and the SMP of low temperature superconductors at high fields.

#### IV. CONCLUSION

In summary, we have systematically studied three  $\text{RbCa}_2\text{Fe}_4\text{As}_4\text{F}_2$  single crystals that have almost the same  $T_c \sim 31$  K but with different amounts of disorder/defects. Only the sample S2 with moderate disorder/defects shows significant SMP effect, although their

self-field  $J_c$  are basically similar. This result manifests the importance of a certain amount of disorder/defects in the formation of SMP. The evolution of the normalized pinning force density demonstrates the type of pinning changing from the dominant density weak pinning at low temperatures to strong pinning at high temperatures. Some expanded  $\text{Ca}_2\text{F}_2$  layers and dislocation defects in  $\text{RbFe}_2\text{As}_2$  layers may be the main cause of non-monotonic SMP phenomenon. The step-like transition of anomalous SMP connects the SMP of high temperature superconductors and that of low temperature superconductors, revealing the possible universal origin related to the E-P phase transition.

#### ACKNOWLEDGMENTS

This work was supported by the Strategic Priority Research Program (B) of the Chinese Academy of Sciences (Grant No. XDB25000000), the National Key R&D Program of China (Grant No. 2018YFA0704300), the National Natural Science Foundation of China (Grant Nos. 12204265 and 12204487), and the Fundamental Research Funds for the Central Universities.

Xiaolei Yi and Xiangzhuo Xing contributed equally to this work.

- 
- [1] G. Blatter, M. V. Feigel'man, B. B. Geshkenbein, A. I. Larkin, and V. M. Vinokur, Vortices in high-temperature superconductors, *Rev. Mod. Phys.* **66**, 1125 (1994).
- [2] Y. Yeshurun, A. P. Malozemoff, and A. Shaulov, Magnetic relaxation in high-temperature superconductors, *Rev. Mod. Phys.* **68**, 911 (1996).
- [3] A. B. Pippard, A possible mechanism for the peak effect in type II superconductors, *Philos. Mag.* **19**, 217 (1969).
- [4] A. I. Larkin and Y. N. Ovchinnikov, Pinning in type II superconductors, *J. Low Temp. Phys.* **34**, 409 (1979).
- [5] B. Rosenstein, B. Y. Shapiro, I. Shapiro, Y. Bruckental, A. Shaulov, and Y. Yeshurun, Peak effect and square-to-rhombic vortex lattice transition in  $\text{La}_{2-x}\text{Sr}_x\text{CuO}_4$ , *Phys. Rev. B* **72**, 144512 (2005).
- [6] A. K. Pramanik, L. Harnagea, C. Nacke, A. U. B. Wolter, S. Wurmehl, V. Kataev, and B. Buchner, Fishtail effect and vortex dynamics in  $\text{LiFeAs}$  single crystals, *Phys. Rev. B* **83**, 094502 (2011).
- [7] R. Kopeliansky, A. Shaulov, B. Y. Shapiro, Y. Yeshurun, B. Rosenstein, J. J. Tu, L. J. Li, G. H. Cao, and Z. A. Xu, Possibility of vortex lattice structural phase transition in the superconducting pnictide  $\text{Ba}(\text{Fe}_{0.925}\text{Co}_{0.075})_2\text{As}_2$ , *Phys. Rev. B* **81**, 092504 (2010).
- [8] Y. Abulafia, A. Shaulov, Y. Wolfus, R. Prozorov, L. Burlachkov, Y. Yeshurun, D. Majer, E. Zeldov, H. Wuhl, V. B. Geshkenbein, and V. M. Vinokur, Plastic Vortex Creep in  $\text{YBa}_2\text{Cu}_3\text{O}_{7-x}$  Crystals, *Phys. Rev. Lett.* **77**, 1596 (1996).
- [9] R. Prozorov, N. Ni, M. A. Tanatar, V. G. Kogan, R. T. Gordon, C. Martin, E. C. Blomberg, P. Prommapan, J. Q. Yan, S. L. Bud'ko, and P. C. Canfield, Vortex phase diagram of  $\text{Ba}(\text{Fe}_{0.93}\text{Co}_{0.07})_2\text{As}_2$  single crystals, *Phys. Rev. B* **78**, 224506 (2008).
- [10] T. Nishizaki, T. Naito, S. Okayasu, A. Iwase, and N. Kobayashi, Effects of weak point disorder on the vortex matter phase diagram in untwinned  $\text{YBa}_2\text{Cu}_3\text{O}_y$  single crystals, *Phys. Rev. B* **61**, 3649 (2000).
- [11] S. Ishida, A. Iyo, H. Ogino, H. Eisaki, N. Takeshita, K. Kawashima, K. Yanagisawa, Y. Kobayashi, K. Kimoto, H. Abe, M. Imai, J.-i. Shimoyama, and M. Eisner, Unique defect structure and advantageous vortex pinning properties in superconducting  $\text{CaKFe}_4\text{As}_4$ , *npj Quantum Mater.* **4**, 27 (2019).
- [12] Y. Pan, W. Zhou, J. Feng, X. Yi, C. Xu, M. Wang, N. Zhou, and Z. Shi, Vortex phase diagram in 1111-type  $\text{CaFe}_{0.89}\text{Co}_{0.11}\text{AsF}$  single crystal, *Supercon. Sci. Technol.* **35**, 025007 (2021).
- [13] I. F. Llovo, D. Sonora, J. Mosqueira, S. Salem-Sugui Jr, S. Sundar, A. D. Alvarenga, T. Xie, C. Liu, S. L. Li, and H. Q. Luo, Vortex dynamics and second magnetization peak in the iron-pnictide superconductor  $\text{Ca}_{0.82}\text{La}_{0.18}\text{Fe}_{0.96}\text{Ni}_{0.04}\text{As}_2$ , *Supercon. Sci. Technol.* **34**, 115010 (2021).
- [14] S. Eley, R. Willa, M. K. Chan, E. D. Bauer, and L. Civale, Vortex phases and glassy dynamics in the highly anisotropic superconductor  $\text{HgBa}_2\text{CuO}_{4+\delta}$ , *Sci. Rep.* **10**, 10239 (2020).
- [15] B. Keimer, S. A. Kivelson, M. R. Norman, S. Uchida, and J. Zaanen, From quantum matter to high-temperature superconductivity in copper oxides, *Nature* **518**, 179 (2015).
- [16] X. Luo and X. Chen, Crystal structure and phase dia-

- grams of iron-based superconductors, *Sci. China Mater.* **58**, 77 (2015).
- [17] C. J. van der Beek, M. Konczykowski, S. Kasahara, T. Terashima, R. Okazaki, T. Shibauchi, and Y. Matsuda, Quasiparticle scattering induced by charge doping of iron-pnictide superconductors probed by collective vortex pinning, *Phys. Rev. Lett.* **105**, 267002 (2010).
- [18] C. J. van der Beek, M. Konczykowski, A. Abal'osheva, I. Abal'osheva, P. Gierlowski, S. J. Lewandowski, M. V. Indenbom, and S. Barbanera, Strong pinning in high-temperature superconducting films, *Phys. Rev. B* **66**, 024523 (2002).
- [19] M. V. Feigel'man, V. B. Geshkenbein, A. I. Larkin, and V. M. Vinokur, Theory of collective flux creep, *Phys. Rev. Lett.* **63**, 2303 (1989).
- [20] Z. C. Wang, C. Y. He, S. Q. Wu, Z. T. Tang, Y. Liu, A. Ablimit, C. M. Feng, and G. H. Cao, Superconductivity in  $\text{KCa}_2\text{Fe}_4\text{As}_4\text{F}_2$  with Separate Double  $\text{Fe}_2\text{As}_2$  Layers, *J. Am. Chem. Soc.* **138**, 7856 (2016).
- [21] R. J. Cava, B. Batlogg, R. B. van Dover, J. J. Krajewski, J. V. Waszczak, R. M. Fleming, W. F. Peck, L. W. Rupp, P. Marsh, A. C. W. P. James, and L. F. Schneemeyer, Superconductivity at 60 K in  $\text{La}_{2-x}\text{Sr}_x\text{CaCu}_2\text{O}_6$ : the simplest double-layer cuprate, *Nature* **345**, 602 (1990).
- [22] J. M. Tarascon, Y. Le Page, P. Barboux, B. G. Bagley, L. H. Greene, W. R. McKinnon, G. W. Hull, M. Giroud, and D. M. Hwang, Crystal substructure and physical properties of the superconducting phase  $\text{Bi}_4(\text{Sr},\text{Ca})_6\text{Cu}_4\text{O}_{16+x}$ , *Phys. Rev. B* **37**, 9382 (1988).
- [23] S. Pyon, Y. Kobayashi, A. Takahashi, W. Li, T. Wang, G. Mu, A. Ichinose, T. Kambara, A. Yoshida, and T. Tamegai, Anisotropic physical properties and large critical current density in  $\text{KCa}_2\text{Fe}_4\text{As}_4\text{F}_2$  single crystal, *Phys. Rev. Mater.* **4**, 104801 (2020).
- [24] X. Yi, M. Li, X. Xing, Y. Meng, C. Zhao, and Z. Shi, Single crystal growth and effects of Ni doping on the novel 12442-type iron-based superconductor  $\text{RbCa}_2\text{Fe}_4\text{As}_4\text{F}_2$ , *New J. Phys.* **22**, 073007 (2020).
- [25] W. Hong, L. Song, B. Liu, Z. Li, Z. Zeng, Y. Li, D. Wu, Q. Sui, T. Xie, S. Danilkin, H. Ghosh, A. Ghosh, J. Hu, L. Zhao, X. Zhou, X. Qiu, S. Li, and H. Luo, Neutron Spin Resonance in a Quasi-Two-Dimensional Iron-Based Superconductor, *Phys. Rev. Lett.* **125**, 117002 (2020).
- [26] T. Wang, J. Chu, H. Jin, J. Feng, L. Wang, Y. Song, C. Zhang, X. Xu, W. Li, Z. Li, T. Hu, D. Jiang, W. Peng, X. Liu, and G. Mu, Single-Crystal Growth and Extremely High  $H_{c2}$  of 12442-Type Fe-Based Superconductor  $\text{KCa}_2\text{Fe}_4\text{As}_4\text{F}_2$ , *J. Phys. Chem. C* **123**, 13925 (2019).
- [27] Z.-C. Wang, Y. Liu, S.-Q. Wu, Y.-T. Shao, Z. Ren, and G.-H. Cao, Giant anisotropy in superconducting single crystals of  $\text{CsCa}_2\text{Fe}_4\text{As}_4\text{F}_2$ , *Phys. Rev. B* **99**, 144501 (2019).
- [28] X. Xing, X. Yi, M. Li, Y. Meng, G. Mu, J.-Y. Ge, and Z. Shi, Vortex phase diagram in 12442-type  $\text{RbCa}_2\text{Fe}_4\text{As}_4\text{F}_2$  single crystal revealed by magnetotransport and magnetization measurements, *Supercon. Sci. Technol.* **33**, 114005 (2020).
- [29] C. P. Bean, Magnetization of High-Field Superconductors, *Rev. Mod. Phys.* **36**, 31 (1964).
- [30] Z. Wang, C. He, Z. Tang, S. Wu, and G. Cao, Crystal structure and superconductivity at about 30 K in  $\text{ACa}_2\text{Fe}_4\text{As}_4\text{F}_2$  ( $A = \text{Rb}, \text{Cs}$ ), *Sci. China Mater.* **60**, 83 (2016).
- [31] Z.-C. Wang, C.-Y. He, S.-Q. Wu, Z.-T. Tang, Y. Liu, and G.-H. Cao, Synthesis, Crystal Structure and Superconductivity in  $\text{RbLn}_2\text{Fe}_4\text{As}_4\text{O}_2$  ( $\text{Ln} = \text{Sm}, \text{Tb}, \text{Dy}, \text{and Ho}$ ), *Chem. Mater.* **29**, 1805 (2017).
- [32] Y. N. Ovchinnikov and B. I. Ivlev, Pinning in layered inhomogeneous superconductors, *Phys. Rev. B* **43**, 8024 (1991).
- [33] N. Haberkorn, J. Kim, S. Suarez, J.-H. Lee, and S. H. Moon, Influence of random point defects introduced by proton irradiation on the flux creep rates and magnetic field dependence of the critical current density  $J_c$  of co-evaporated  $\text{GdBa}_2\text{Cu}_3\text{O}_{7-\delta}$  coated conductors, *Supercon. Sci. Technol.* **28**, 125007 (2015).
- [34] N. Haberkorn, M. Xu, W. R. Meier, J. Schmidt, S. L. Bud'ko, and P. C. Canfield, Effect of Ni doping on vortex pinning in  $\text{CaK}(\text{Fe}_{1-x}\text{Ni}_x)_4\text{As}_4$  single crystals, *Phys. Rev. B* **100**, 064524 (2019).
- [35] D. Dew-Hughes, Flux pinning mechanisms in type II superconductors, *Philos. Mag.* **30**, 293 (1974).
- [36] M. R. Koblishka, A. J. J. van Dalen, T. Higuchi, S. I. Yoo, and M. Murakami, Analysis of pinning in  $\text{NdBa}_2\text{Cu}_3\text{O}_{7-\delta}$  superconductors, *Phys. Rev. B* **58**, 2863 (1998).
- [37] H. Yang, H. Luo, Z. Wang, and H.-H. Wen, Fishtail effect and the vortex phase diagram of single crystal  $\text{Ba}_{0.6}\text{K}_{0.4}\text{Fe}_2\text{As}_2$ , *Appl. Phys. Lett.* **93**, 142506 (2008).
- [38] W. Zhou, X. Xing, W. Wu, H. Zhao, and Z. Shi, Second magnetization peak effect, vortex dynamics, and flux pinning in 112-type superconductor  $\text{Ca}_{0.8}\text{La}_{0.2}\text{Fe}_{1-x}\text{Co}_x\text{As}_2$ , *Sci. Rep.* **6**, 22278 (2016).
- [39] D. L. Sun, Y. Liu, and C. T. Lin, Comparative study of upper critical field  $H_{c2}$  and second magnetization peak/Hspin hole- and electron-doped  $\text{BaFe}_2\text{As}_2$  superconductor, *Phys. Rev. B* **80**, 144515 (2009).
- [40] D. Van Gennep, A. Hassan, H. Luo, and M. Abdel-Hafiez, Sharp peak of the critical current density in  $\text{BaFe}_{2-x}\text{Ni}_x\text{As}_2$  at optimal composition, *Phys. Rev. B* **101**, 235163 (2020).
- [41] M. Shahbazi, X. L. Wang, K. Y. Choi, and S. X. Dou, Flux pinning mechanism in  $\text{BaFe}_{1.9}\text{Ni}_{0.1}\text{As}_2$  single crystals: Evidence for fluctuation in mean free path induced pinning, *Appl. Phys. Lett.* **103**, 032605 (2013).
- [42] J. Tao, Q. Deng, H. Yang, Z. Wang, X. Zhu, and H.-H. Wen, Magnetization relaxation, critical current density, and vortex dynamics in a  $\text{Ba}_{0.66}\text{K}_{0.32}\text{BiO}_{3+\delta}$  single crystal, *Phys. Rev. B* **91**, 214516 (2015).
- [43] N. Kokubo, K. Kadowaki, and K. Takita, Peak effect and dynamic melting of vortex matter in  $\text{NbSe}_2$  crystals, *Phys. Rev. Lett.* **95**, 177005 (2005).
- [44] Y. Jiao, W. Cheng, Q. Deng, H. Yang, and H.-H. Wen, Collective vortex pinning and merging of the irreversibility line and second peak effect in optimally doped  $\text{Ba}_{1-x}\text{K}_x\text{BiO}_3$  single crystals, *Physica C* **545**, 43 (2018).
- [45] T. Nishizaki, T. Naito, and N. Kobayashi, Anomalous magnetization and field-driven disordering transition of a vortex lattice in untwinned  $\text{YBa}_2\text{Cu}_3\text{O}_y$ , *Phys. Rev. B* **58**, 11169 (1998).
- [46] C. Wang, T. He, Q. Han, C. Fan, Q. Tang, D. Chen, Q. Lei, S. Sun, Y. Li, and B. Yu, Novel sample-thickness-dependent flux pinning behaviors of  $\text{KFe}_2\text{As}_2$  intercalations in  $\text{CaKFe}_4\text{As}_4$  single crystals, *Supercon. Sci. Technol.* **34**, 055001 (2021).
- [47] A. Ichinose, S. Pyon, T. Tamegai, and S. Ishida, Elucidating the origin of planar defects that enhance critical current density in  $\text{CaKFe}_4\text{As}_4$  single crystals, *Supercon.*



- Sci. Technol.* **34**, 034003 (2021).
- [48] S. Pyon, A. Takahashi, I. Veshchunov, T. Tamegai, S. Ishida, A. Iyo, H. Eisaki, M. Imai, H. Abe, T. Terashima, and A. Ichinose, Large and significantly anisotropic critical current density induced by planar defects in  $\text{CaKFe}_4\text{As}_4$  single crystals, *Phys. Rev. B* **99**, 104506 (2019).
- [49] S. J. Singh, M. Bristow, W. R. Meier, P. Taylor, S. J. Blundell, P. C. Canfield, and A. I. Coldea, Ultrahigh critical current densities, the vortex phase diagram, and the effect of granularity of the stoichiometric high- $T_c$  superconductor  $\text{CaKFe}_4\text{As}_4$ , *Phys. Rev. Mater.* **2**, 074802 (2018).
- [50] Y. Sun, S. Pyon, T. Tamegai, R. Kobayashi, T. Watashige, S. Kasahara, Y. Matsuda, and T. Shibauchi, Critical current density, vortex dynamics, and phase diagram of single-crystal FeSe, *Phys. Rev. B* **92**, 144509 (2015).
- [51] M. Bonura, E. Giannini, R. Vienneis, and C. Senatore, Temperature and time scaling of the peak-effect vortex configuration in  $\text{FeTe}_{0.7}\text{Se}_{0.3}$ , *Phys. Rev. B* **85**, 134532 (2012).
- [52] S. Salem-Sugui, L. Ghivelder, A. D. Alvarenga, L. F. Cohen, K. A. Yates, K. Morrison, J. L. Pimentel, H. Luo, Z. Wang, and H.-H. Wen, Flux dynamics associated with the second magnetization peak in the iron pnictide  $\text{Ba}_{1-x}\text{K}_x\text{Fe}_2\text{As}_2$ , *Phys. Rev. B* **82**, 054513 (2010).
- [53] M. Polichetti, A. Galluzzi, K. Buchkov, V. Tomov, E. Nazarova, A. Leo, G. Grimaldi, and S. Pace, A precursor mechanism triggering the second magnetization peak phenomenon in superconducting materials, *Sci. Rep.* **11**, 7247 (2021).
- [54] H. Yang, C. Ren, L. Shan, and H.-H. Wen, Magnetization relaxation and collective vortex pinning in the Fe-based superconductor  $\text{SmFeAsO}_{0.9}\text{F}_{0.1}$ , *Phys. Rev. B* **78**, 092504 (2008).
- [55] B. Shen, P. Cheng, Z. Wang, L. Fang, C. Ren, L. Shan, and H.-H. Wen, Flux dynamics and vortex phase diagram in  $\text{Ba}(\text{Fe}_{1-x}\text{Co}_x)_2\text{As}_2$  single crystals revealed by magnetization and its relaxation, *Phys. Rev. B* **81**, 014503 (2010).
- [56] S. Yue, T. Toshihiro, T. Yuji, P. Suneng, S. Zhixiang, and T. Tsuyoshi, Magnetic relaxation and collective vortex creep in  $\text{FeTe}_{0.6}\text{Se}_{0.4}$  single crystal, *EPL* **103**, 57013 (2013).
- [57] A. K. Pramanik, L. Harnagea, S. Singh, S. Aswartham, G. Behr, S. Wurmehl, C. Hess, R. Klingeler, and B. Buchner, Critical current and vortex dynamics in single crystals of  $\text{Ca}(\text{Fe}_{1-x}\text{Co}_x)_2\text{As}_2$ , *Phys. Rev. B* **82**, 014503 (2010).